Metal Nanoparticles

Deutsche Ausgabe: DOI: 10.1002/ange.201502012
Internationale Ausgabe: DOI: 10.1002/anie.201502012

Reversible Modulation of Surface Plasmons in Gold Nanoparticles Enabled by Surface Redox Chemistry**

Zheng Li, Jonathan J. Foley IV, Sheng Peng, Cheng-Jun Sun, Yang Ren, Gary P. Wiederrecht, Stephen K. Gray,* and Yugang Sun**

Abstract: *Switchable surface redox chemistry is demonstrated in gold@iron/iron oxide core–shell nanoparticles with ambient oxidation and plasmon-mediated reduction to modulate the oxidation state of shell layers. The iron shell can be oxidized to iron oxide through ambient oxidation, leading to an enhancement and red-shift of the gold surface plasmon resonance (SPR). This enhanced gold SPR can drive reduction of the iron oxide shell under broadband illumination to reversibly blue-shift and significantly dampen gold SPR absorption. The observed phenomena provide a unique mechanism for controlling the plasmonic properties and surface chemistry of small metal nanoparticles.*

Collective oscillations of conduction electrons excited by incident light, known as surface plasmon resonance (SPR), are responsible for the extraordinary optical properties of noble metal nanostructures.[1] SPR enables extreme confinement of optical energy in the vicinity of a plasmonic structure, which can strongly enhance light–matter interactions in the near-field of the plasmon. This enhancement leads to the exceptional environmental sensitivity of the SPR and provides the foundation for a variety of sensing applications.[2] Furthermore, the near-field enhancement associated with SPR can enhance Rayleigh scattering, Raman scattering, and fluorescence efficiency of molecules adsorbed on plasmonic nanostructures,[3] enabling spectroscopic sensitivity down to the single-molecule limit.[4] Since the SPR characteristics of nanostructures are dependent on their size, shape, composition, and surrounding environment,[5] a plethora of methods have been developed to synthesize noble metal nanoparticles with tunable parameters to tailor their optical properties.[6] For instance, hybridization of plasmonic metal nanoparticles with ferromagnetic or semiconductor materials can effectively influence their optical properties through magneto-plasmonic interferometry and light-driven injection of charge carriers from semiconductors to metals, respectively.[7] Recent investigations also show the potential of surface plasmons (SPs) to drive chemical reactions,[8] for example, the reduction of Cu_2O to Cu in $Cu@Cu_2O$ core–shell particles.[9]

Herein, we report self-modulation of the plasmonic properties of core–shell nanoparticles composed of Au, Fe, and iron oxide (FeO_x). Alternating the oxidation states of iron through plasmon-mediated reduction and ambient oxidation enables the reversible damping and recovery of the SPR signal of the Au core nanoparticles. To our knowledge, this work represents a novel approach and the first demonstration of utilizing external stimuli (SPR-mediated photoillumination and oxidizing atmosphere) to reversibly switch the oxidation states of shell materials, and reciprocally the SPR properties of hybrid core–shell nanostructures.

The $Au@Fe@FeO_x$ core–shell nanoparticles are synthesized through a seed-mediated approach[10] in which uniform Au nanoparticles are used as seeds (see the Supporting Information for details).[11] The thickness of the shells monotonically increases with increasing reaction time (Figure 1 B–F). Iron is readily oxidized to magnetite (Fe_3O_4) and maghemite (γ-Fe_2O_3) once the samples are exposed to the ambient atmosphere.[12] The outermost Fe atoms tend to be converted into Fe_2O_3, which has a higher oxidation state than the Fe_3O_4 layer that tends to reside closer to the Au core.[13] As a result, particles with a thick shell coating that is partially oxidized consist of Au cores, Fe shells, and FeO_x shells (see color illustrative insets in Figure 1). The detailed compositions of the core–shell nanoparticles were analyzed using X-ray absorption near-edge structure (XANES) spectroscopy, and the results are presented in the Supporting Information, Table S1.

UV/Vis absorption spectroscopy was employed to elucidate the variation of optical properties of the $Au@Fe@FeO_x$ core–shell nanoparticles with different shell compositions. As shown in Figure 2 A, the bare Au nanoparticles (Figure 1 A) dispersed in toluene exhibit a well-defined absorption peak with a maximum at 520 nm. The core–shell nanoparticles formed at short deposition times (1 min and 2 min with the corresponding samples shown in Figure 1 B and C) are

[*] Dr. Z. Li,[+] Dr. J. J. Foley IV,[+] Dr. S. Peng, Dr. G. P. Wiederrecht, Dr. S. K. Gray, Dr. Y. Sun
Center for Nanoscale Materials, Argonne National Laboratory
9700 South Cass Avenue, Argonne, IL 60439 (USA)
E-mail: wiederrecht@anl.gov
gray@anl.gov
ygsun@anl.gov
Dr. C.-J. Sun, Dr. Y. Ren
X-ray Science Division, Advanced Photon Source
Argonne National Laboratory (USA)
[+] These authors contributed equally to this work.

[**] This work was performed at the Center for Nanoscale Materials, a U.S. Department of Energy, Office of Science, Office of Basic Energy Sciences User Facility under Contract no. DE-AC02-06CH11357. PNC/XSD facilities at the Advanced Photon Source, and research at these facilities, are supported by the US Department of Energy—Basic Energy Sciences, the Canadian Light Source and its funding partners, the University of Washington, and the Advanced Photon Source. Use of the Advanced Photon Source, an Office of Science User Facility operated for the U.S. Department of Energy (DOE) Office of Science by Argonne National Laboratory, was supported by the U.S. DOE under Contract No. DE-AC02-06CH11357.

Supporting information for this article is available on the WWW under http://dx.doi.org/10.1002/anie.201502012.

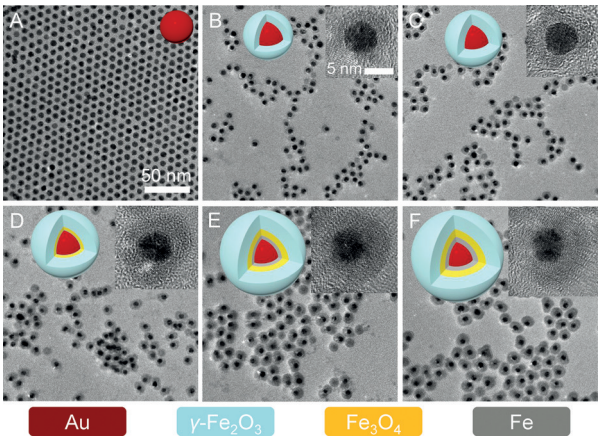

Figure 1. TEM and HRTEM (inset) images of Au nanoparticles A) before and B)–F) after their surfaces were coated with iron-containing shells grown for different times: B) 1 min, C) 2 min, D) 5 min, E) 20 min, and F) 30 min. The color illustrative insets show the compositional construction of different core–shell nanoparticles. The thicknesses of layers with different iron-containing compositions can be found in the Supporting Information, Table S1. Scale bars in the image of (A) and inset of (B) apply to all the other images and insets, respectively.

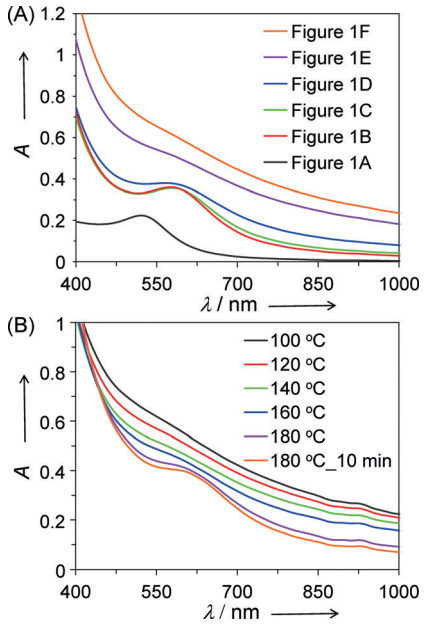

Figure 2. Quantitative UV/Vis spectra of A) Au nanocrystals during the deposition of iron-containing shells at different times and B) oxidation of Au@Fe@FeO_x nanoparticles, which grew for 30 min in (A), through air bubbling oxidation in which the sample was heated at 180 °C in ODE with controlled air bubbling speed at 80 mL min^{-1}.

composed of Au cores and γ-Fe_2O_3 shells, and their absorption spectra exhibit red-shifted SPR. The core–shell nanoparticles formed at deposition times beyond 5 min (Figure 1 D–F) are composed of shells containing metallic Fe in direct contact with the Au cores. The corresponding absorption spectra show a significant damping of the peak feature. The Au SPR absorption band becomes completely featureless for core–shell nanoparticles formed at long deposition times (for example, 30 min).

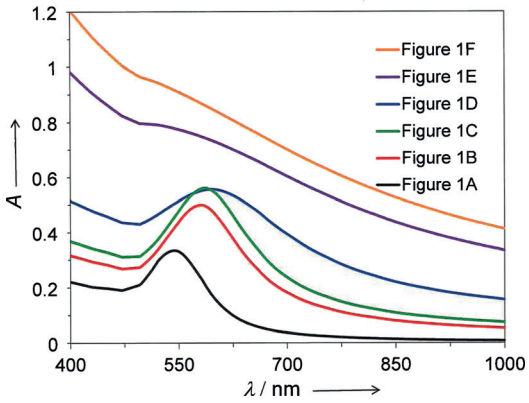

Figure 3. Theoretical calculation results of UV/Vis spectra based upon the composition evolution during the growth of iron-containing shells on Au nanoparticle core (see color illustrative insets in Figure 1).

Rigorous electrodynamics calculations have been performed to correlate the observed changes in the absorption spectra with the changes in composition and oxidation state of the iron-containing shells in the Au@Fe@FeO_x nanoparticles (Figure 3). Mie theory analysis in the quasi-static limit is used to write an expression for the SPR condition of an Au@Fe core–shell particle in terms of the radii and permittivity of the core and shell layers, as well as the permittivity of the surrounding media.[14] This analysis reveals that the strong broadband absorption of metallic Fe is responsible for the dramatic damping of the Au SPR feature. It can be seen that a Fe layer as thin as 0.5 nm around an Au nanoparticle completely destroys the condition for SPR in the core–shell structures (Supporting Information, Figure S1). Significantly lower near-field intensity is also observed at the Au SPR frequency in the Fe coated particles (Supporting Information, Figure S2). The ratio of the shell thickness to the core particle radius is important to determine the SPR damping efficiency, and so thicker Fe shells would be required to produce such dramatic damping for larger Au particles (Supporting Information, Figure S3). A more detailed discussion of the damping mechanism is provided in the Supporting Information. This result is fully consistent with the experimental observation of extreme damping of the absorption peak in the core–shell particles formed at long deposition times, which contain metallic Fe in the shells. Calculations on all of the Au@FeO_x structures reveal that the SPR peak position is red-shifted in the presence of the oxide layer, consistent with the experimentally observed evolution of the absorption spectra taken at short deposition times.

The profound damping effect of metallic Fe on the Au SPR peak can be reversed by deeply oxidizing the sample to convert the Fe into FeO_x, leading to the regeneration of the Au SPR peak. For example, heating the Au@Fe@FeO_x core–shell nanoparticles (Figure 1 F) under air bubbling oxidation (see the Supporting Information for details), can transform the innermost Fe into FeO_x. Corresponding XANES analysis (Supporting Information, Table S1) over the samples confirms a complete conversion of Fe into FeO_x and the formation of Au@FeO_x core–shell particles. TEM images of the sample formed after oxidation (Supporting Information,

Figure S4) indicate that the original morphology remains. As shown in Figure 2B, the characteristic Au SPR feature reemerges after the solution is heated and held at 180 °C. Besides, the complete transformation of Fe into FeO_x coincides with the recovery of the Au SPR peak. The experimental measurements in Figure 2 and the calculated results in Figure 3 are consistent with our conjecture that formation of the Fe layer around the Au core plays a fundamental role in triggering the damping of the Au SPR feature, and that the SPR damping can be reversed by transforming Fe to FeO_x.

To demonstrate plasmon-mediated reduction of iron oxide, we start with Au@FeO_x core–shell nanoparticles that are composed of a thin iron oxide layer and exhibit a typical Au SPR peak with strong intensity (see the Supporting Information for details). Decay of the Au SPs results in a distribution of hot electrons that can drive the reduction of FeO_x adjacent to the Au surfaces to form Fe.[8,9,14,15] To prevent re-oxidation or hot-electron scavenging, experiments demonstrating this effect are carried out with a freeze–pump–thaw (FPT) cell (Supporting Information, Figure S5) to remove the dissolved oxygen. As shown in Figure 4A, illumination with a bright white light source leads to a reduction in the SPR peak height (see definition in Figure 4 caption), with longer illumination times leading to greater reduction in the peak intensity. The SPR peak recovers when the FPT cell is opened to ambient oxidation. As shown in Figure 4B, with the Au SPR peak maximum at the same absorbance, the left valley of the Au SPR peak gradually shifts to lower absorbance when the exposure time to ambient oxidation increases. The reversible damping/recovery of the Au SPR strength can be repeated by alternatively exposing the core–shell nanoparticles to white light under inert atmosphere, and subsequently, to ambient oxidation (Figure 4C; Supporting Information, Figures S6 and S9). The SPR peak position is also reversibly shifted during cycles between light illumination and ambient oxidation. As shown in Figure 4D, the Au SPR peak progressively blue-shifts with light illumination time, and subsequent ambient oxidation progressively shifts the SPR peak to the red. The fatigue, that is, the variation of peak height and intensities during cycles, could be due to the subtle morphological variation of the Fe/FeO_x shells, which can influence the optical properties of the core–shell nanostructure.

To further correlate the iron composition with optical properties, the oxidation states of the iron-containing shells are monitored with XANES spectroscopy of representative samples in Kapton tubes (Supporting Information, Figure S7) during the cycle of light illumination/ambient oxidation. As shown in the Supporting Information, Figure S8 (analysis in caption), light illumination induces reduction of FeO_x to form Fe, and exposure to ambient oxidation transforms metallic Fe back to FeO_x. Theoretical calculations (Supporting Information, Figure S9) unambiguously shows the continuous blue-shifting and dampening of Au SPR with the increase of Fe composition in the shell. Accordingly, the blue-shift and intensity decrease of the Au SPR peak during light illumination under inert atmosphere can be attributed to the formation of metallic Fe around the Au cores, and oxidation of Fe induces the red-shift and intensity increase of the Au SPR peak during ambient oxidation.

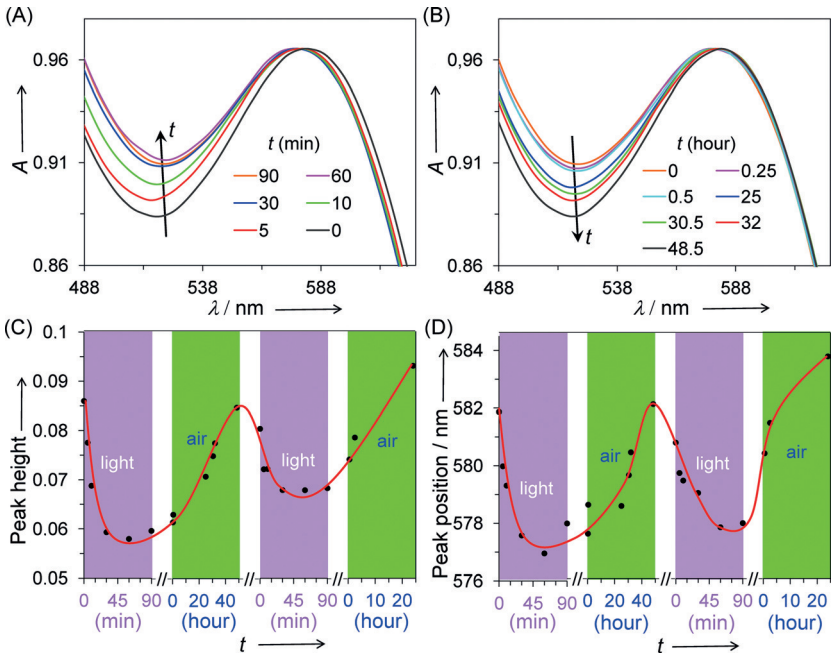

Figure 4. UV/Vis absorption spectra of Au@FeO_x core–shell nanoparticles (A) after shining with white light in the FPT cell for varied times, and (B) followed by exposing to ambient oxidation for different times. The y-axes of the spectra are aligned against the peak absorbance of the Au SPR. The full-range UV/Vis spectra can be found in the Supporting Information, Figure S6A,B. Evolution of C) peak height and D) peak position of the Au SPR during two cycles of alternating light illumination and ambient oxidation. The corresponding UV/Vis spectra recorded in the second cycle are presented in the Supporting Information, Figure S6C,D. The peak heights are defined by subtracting the Au SPR peak absorbance with the absorbance value at the left valley position. The red curves in (C) and (D) are only to guide the eye.

The dynamics during plasmon-mediated reduction of FeO_x are further studied by transient absorption (TA) spectroscopy. Two representative samples, namely Au@FeO_x nanoparticles oxidized in ambient oxidation and the same sample after photoreduction, are presented as oxidized and reduced core–shell nanoparticles for simplicity. After the excitation pulse near the SPR peak position (that is, 582 ± 6 nm), the oxidized core–shell nanoparticles in Figure 5A exhibit asymmetric photoinduced absorption (PA) spectra with strong signals at the blue side of the SPR peak position and negligible signal at the red side of the SPR peak position. This corresponds to a blue-shift of the SPR peak position after resonant excitation, brought about by the reduction of FeO_x. In contrast, for the reduced core–shell nanoparticles, the PA spectra are more symmetric, as shown in Figure 5B. Especially at a delay time of 1.33 ps, the features for this sample are almost the same as pure Au nanoparticles,

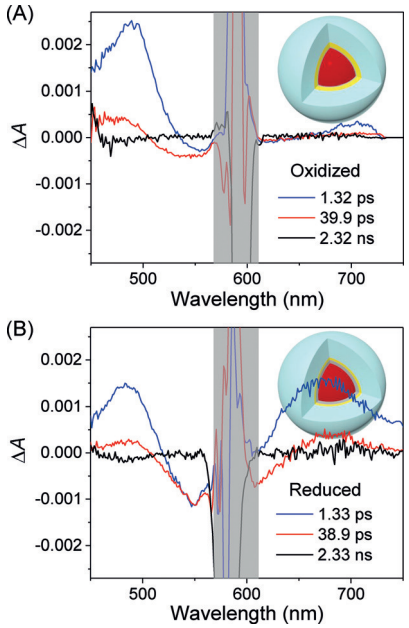

Figure 5. Transient absorption (TA) spectra of A) oxidized and B) reduced core–shell nanoparticles excited with a laser of 588 nm. The insets illustrate the corresponding compositional constructions of the core–shell nanoparticles using the same color scheme as in Figure 1.

with a bleach at the resonance position and similar PA intensity at both sides of the SPR peak position.[16] The divergent TA features from oxidized and reduced core–shell nanoparticles suggest that hot electrons are likely injected into the shells of the oxidized core–shell nanoparticles to reduce FeO_x into Fe, leading to a dramatic change of the relaxation dynamics of the excited Au SPs. Hence, we conclude that the Au SPR is the actual source of hot electrons for the reduction of FeO_x layer during light illumination.

In summary, we have demonstrated a reversible self-modulation of optical properties of Au@FeO_x core–shell nanoparticles by alternating cycles of plasmon-mediated reduction of FeO_x into Fe and ambient oxidation of Fe back into FeO_x. Combining the investigations from UV/Vis absorption spectroscopy, XANES spectroscopy, transient absorption kinetics, and theoretical calculations, we reveal that reducing FeO_x into Fe around the Au nanoparticle in Au@FeO_x core–shell nanoparticles is responsible for the damping of the Au SPR peak intensity and the blue-shift of the SPR peak position, and that the backward oxidation of Fe into FeO_x conversely recover the intensity and position of the Au SPR peak. Optimization of the sample composition and operational environment should increase the extent of reversible modulation of the metal SPR, given the current limitation on penetration depth of hot electrons and air-tight nature of the cell. For example, stronger plasmonic materials, such as silver, may be more efficacious in altering the oxidation state of shell layers under illumination conditions. Correspondingly, stronger SPR modulation should be observed in this system, as theoretically predicted for the Ag@Fe@FeO_x core–shell nanostructure (Supporting Information, Figure S10). To conclude, our results pave the way for convenient and reversible control of the surface plasmon properties in metal nanoparticles by making use of surface redox chemistry.

Keywords: core–shell nanoparticles · gold nanocrystals · iron · surface plasmon resonance · surface redox chemistry

How to cite: *Angew. Chem. Int. Ed.* **2015**, *54*, 8948–8951
Angew. Chem. **2015**, *127*, 9076–9079

[1] P. W. Atkins, J. De Paula, *Atkins' Physical chemistry*, Oxford University Press, Oxford, **2014**, pp. 944–945.
[2] a) K. A. Willets, R. P. Van Duyne, *Annu. Rev. Phys. Chem.* **2007**, *58*, 267; b) J. N. Anker, W. P. Hall, O. Lyandres, N. C. Shah, J. Zhao, R. P. Van Duyne, *Nat. Mater.* **2008**, *7*, 442; c) P. K. Jain, X. Huang, I. H. El-Sayed, M. A. El-Sayed, *Acc. Chem. Res.* **2008**, *41*, 1578.
[3] S. Eustis, M. A. El-Sayed, *Chem. Soc. Rev.* **2006**, *35*, 209.
[4] a) S. Nie, S. R. Emory, *Science* **1997**, *275*, 1102; b) K. Kneipp, Y. Wang, H. Kneipp, L. T. Perelman, I. Itzkan, R. Dasari, M. S. Feld, *Phys. Rev. Lett.* **1997**, *78*, 1667.
[5] a) P. Mulvaney, *Langmuir* **1996**, *12*, 788; b) K. L. Kelly, E. Coronado, L. L. Zhao, G. C. Schatz, *J. Phys. Chem. B* **2003**, *107*, 668; c) G. V. Hartland, *Chem. Rev.* **2011**, *111*, 3858; d) Y. Sun, S. K. Gray, S. Peng, *Phys. Chem. Chem. Phys.* **2011**, *13*, 11814.
[6] a) X. Lu, M. Rycenga, S. E. Skrabalak, B. Wiley, Y. Xia, *Annu. Rev. Phys. Chem.* **2009**, *60*, 167; b) S. Peng, J. M. McMahon, G. C. Schatz, S. K. Gray, Y. Sun, *Proc. Natl. Acad. Sci. USA* **2010**, *107*, 14530; c) R. Jiang, H. Chen, L. Shao, Q. Li, J. Wang, *Adv. Mater.* **2012**, *24*, OP200; d) Y. Sun, J. J. Foley IV, S. Peng, Z. Li, S. K. Gray, *Nano Lett.* **2013**, *13*, 3958.
[7] a) V. V. Temnov, G. Armelles, U. Woggon, D. Guzatov, A. Cebollada, A. Garcia-Martin, J.-M. Garcia-Martin, T. Thomay, A. Leitenstorfer, R. Bratschitsch, *Nat. Photonics* **2010**, *4*, 107; b) E. Ferreiro-Vila, M. Iglesias, E. Paz, F. J. Palomares, F. Cebollada, J. M. Gonzalez, G. Armelles, J. M. Garcia-Martin, A. Cebollada, *Phys. Rev. B* **2011**, *83*, 205120; c) H. Choi, W. T. Chen, P. V. Kamat, *ACS Nano* **2012**, *6*, 4418.
[8] C. Clavero, *Nat. Photonics* **2014**, *8*, 95.
[9] A. Marimuthu, J. Zhang, S. Linic, *Science* **2013**, *339*, 1590.
[10] E. V. Shevchenko, M. I. Bodnarchuk, M. V. Kovalenko, D. V. Talapin, R. K. Smith, S. Aloni, W. Heiss, A. P. Alivisatos, *Adv. Mater.* **2008**, *20*, 4323.
[11] S. Peng, Y. Lee, C. Wang, H. Yin, S. Dai, S. Sun, *Nano Res.* **2008**, *1*, 229.
[12] a) T. Hyeon, S. S. Lee, J. Park, Y. Chung, H. Bin Na, *J. Am. Chem. Soc.* **2001**, *123*, 12798; b) S. Sun, H. Zeng, D. B. Robinson, S. Raoux, P. M. Rice, S. X. Wang, G. Li, *J. Am. Chem. Soc.* **2004**, *126*, 273; c) K. Woo, J. Hong, S. Choi, H. W. Lee, J. P. Ahn, C. S. Kim, S. W. Lee, *Chem. Mater.* **2004**, *16*, 2814; d) A. Cabot, V. F. Puntes, E. Shevchenko, Y. Yin, L. Balcells, M. A. Marcus, S. M. Hughes, A. P. Alivisatos, *J. Am. Chem. Soc.* **2007**, *129*, 10358; e) E. V. Shevchenko, J. B. Kortright, D. V. Talapin, S. Aloni, A. P. Alivisatos, *Adv. Mater.* **2007**, *19*, 4183.
[13] a) J. Park, E. Lee, N. M. Hwang, M. S. Kang, S. C. Kim, Y. Hwang, J. G. Park, H. J. Noh, J. Y. Kini, J. H. Park, T. Hyeon, *Angew. Chem. Int. Ed.* **2005**, *44*, 2872; *Angew. Chem.* **2005**, *117*, 2932; b) S. Peng, C. Wang, J. Xie, S. Sun, *J. Am. Chem. Soc.* **2006**, *128*, 10676; c) S. Peng, S. Sun, *Angew. Chem. Int. Ed.* **2007**, *46*, 4155; *Angew. Chem.* **2007**, *119*, 4233.
[14] S. K. Cushing, J. Li, F. Meng, T. R. Senty, S. Suri, M. Zhi, M. Li, A. D. Bristow, N. Wu, *J. Am. Chem. Soc.* **2012**, *134*, 15033.
[15] A. O. Govorov, H. Zhang, Y. K. Gun'ko, *J. Phys. Chem. C* **2013**, *117*, 16616.
[16] A. Comin, K. Korobchevskaya, C. George, A. Diaspro, L. Manna, *Nano Lett.* **2012**, *12*, 921.

Received: March 5, 2015
Revised: April 12, 2015
Published online: June 11, 2015

